JOURNAL OF GEOPHYSICAL RESEARCH, VOL. 105, NO. A10, PAGES 23,005–23,014, OCTOBER 1, 2000

Electrostatic potential patterns in the high-latitude ionosphere constrained by SuperDARN measurements

S. G. Shepherd and J. M. Ruohoniemi

Applied Physics Laboratory, Johns Hopkins University, Laurel, Maryland

Abstract. The recent addition of two radars to the existing network of six Super Dual Auroral Radar Network (SuperDARN) HF radars in the Northern Hemisphere has significantly extended the area in the high latitude where measurements of convecting ionospheric plasma are made. We show that the distribution of the electrostatic potential Φ associated with the "$\mathbf{E}\times\mathbf{B}$" drift of ionospheric plasma can be reliably mapped on global scales when velocity measurments provide sufficient coverage. The global convection maps, or the equivalent electrostatic potential maps, are solved using an established technique of fitting velocity data to an expansion of Φ in terms of spherical harmonic functions. When the measurements are extensive, and especially when they span the region between the extrema in the potential distribution, the solution for the global pattern becomes insensitive to the choice of statistical model data used to constrain the fitting. That is, the statistical model data then only guide the solution in regions where no measurements are available, and the details of the model data have little effect on the gross features of the large-scale convection patterns. The resulting total potential variation across the polar cap, Φ_{PC}, is virtually independent of the statistical model. The ability to accurately determine Φ_{PC} and the global potential Φ on the basis of direct measurements is an important step in understanding solar wind-magnetosphere-ionosphere coupling.

1. Introduction

Plasma in the high-latitude ionosphere responds to magnetospheric electric fields resulting from a combination of viscous interactions and magnetic reconnection processes occurring at the magnetopause and in the magnetotail. The resulting large-scale electric fields map along geomagnetic field lines with little attenuation to the ionosphere where they drive plasma convection according to $\mathbf{v} = \mathbf{E}\times\mathbf{B}/B^2$. Measuring the velocity of the convecting ionospheric plasma allows the convection electric field, $\mathbf{E} = -\nabla\Phi$, to be locally determined, where Φ is the electrostatic potential. Such measurements provide insight into solar wind-magnetosphere-ionosphere (SW-M-I) and ionosphere-thermosphere (I-T) coupling processes as well as being valuable for comparison and validation of real-time and predictive space weather models.

While knowledge of Φ over localized regions is useful in some specific studies, a solution of Φ over the entire high-latitude convection region (greater than $\sim 50°\Lambda$) is often desirable, and sometimes required. For example, recent comparisons of global magnetospheric magnetohydrodynamic (MHD) models with indirect measurements of ionospheric electric fields have been made [*Slinker et al.*, 1999]. Differences in derived ionospheric quantities, such as Φ, were observed and used to adjust parameters in the MHD model in order to make the outputs more realistic. Further improvements are possible from comparisons of MHD models with direct measurements of the ionospheric electric fields over the entire convection zone.

The total potential variation across the polar cap, Φ_{PC}, is an important measure of the coupling between the solar wind and the magnetosphere. By accurately determining Φ_{PC} with direct measurements, it is possible to validate several empirical relations between Φ_{PC} and the interplanetary magnetic field (IMF) [e.g., *Reiff et al.*, 1981; *Boyle et al.*, 1997].

With the recent addition of new radars to the Super Dual Auroral Radar Network (SuperDARN) system, an important threshold has been reached, namely, definition of the global characteristics of the high-latitude convection pattern based solely on direct measurements of convection. The purpose of this paper is to demonstrate that definitive global solutions of Φ are now possible with direct measurements. Toward this end, we show that given sufficient coverage, the solution for Φ is insensitive to the selection of statistical model data. The measurements during such periods largely constrain the global solution of Φ and Φ_{PC}, minimizing the impact of the statistical model. Maps of Φ determined using this technique are suitable for SW-M-I

Paper number 2000JA000171.
0148-0227/00/2000JA000171$09.00

and I-T coupling studies and as validation measures for MHD models.

2. Background

Many techniques have been developed to infer the instantaneous state of the electrostatic potential in the high-latitude ionosphere. One common method utilizes electric field measurements from drift meters on low-alititude satellites such as OGO 6, DE 2, and DMSP to construct synoptic maps of Φ [e.g., *Heppner*, 1977; *Heppner and Maynard*, 1987; *Weimer*, 1995]. A drawback to studies of this type is the limited spatial extent of the measurements. Multiple satellite passes are required to produce synoptic or global patterns, which, as a result, become statistical or averaged in nature. Estimation of Φ over the entire high-latitude ionosphere based on a single satellite pass requires either numerous assumptions about the convection at large distances from the satellite track or the liberal use of statistical data.

A procedure called the assimilative mapping of ionospheric electrodynamics (AMIE) technique was developed to overcome such limitations by incorporating a variety of different types of observations. Direct measurements of the convection velocity from radars or satellites are combined with indirect measurements of magnetic variations from magnetometers or satellites to fabricate global maps of electrostatic potential [*Richmond and Kamide*, 1988]. While this technique is widely used for the purpose of constructing maps of Φ over the entire high-latitude region, uncertainties in the specification of ionospheric conductances, necessary in the inversion of magnetograms, can greatly affect the solution. The reliance on magnetometers has been due to the availability of these data over large areas. Recently, it has become possible to base the global solution of Φ more on direct measurements of convection velocity.

Ruohoniemi and Baker [1998] presented a technique comparable to AMIE that is tailored to direct measurements of convection from HF radars. In their approach, line-of-sight (LOS) Doppler velocities from SuperDARN are fitted to an expansion of Φ in terms of spherical harmonic functions. The LOS Doppler velocity measurements of the ionospheric convection velocity provided by SuperDARN are augmented by additional velocity vectors from a statistical model to constrain the solution in regions where no SuperDARN data are available. The statistical model currently used is the Applied Physics Laboratory (APL) convection model, which was derived from nearly 6 years of HF radar observations [*Ruohoniemi and Greenwald*, 1996]. The necessity of using statistical data was discussed by *Ruohoniemi and Baker* [1998], and they point out that any model could be used.

The need for statistical model data can be understood from the following considerations. A best fit global solution for Φ could indeed be determined from a set of localized radar velocity measurements. The solution would be optimal in the sense that the differences between the measured velocities and those implied by the fitting are minimized in a least squares sense. The physical expression of the solution is a set of coefficients for the terms of the spherical harmonic expansion of Φ. Over the area of measurements the values of the coefficients are constrained in such a way as to reproduce the observations. Outside of this area no constraints exist, and straightforward application of the set of coefficients will lead, in general, to wildly unrealistic results for Φ. If a plausible global solution is required, the fitting must be suitably constrained over the outlying areas.

In the fitting algorithm of *Ruohoniemi and Baker* [1998] a pattern from the statistical model is sampled for velocity values that bound the values of the coefficients in the spherical harmonic expansion of Φ. In this way, the solution for Φ beyond the area of radar observations is effectively constrained to realistic values. To increase realism, the selection of model data is keyed to the prevailing IMF conditions at the magnetopause. The fitting with model data is, of course, somewhat less optimal in terms of reproducing the direct measurements of convection velocity. The mapping of Φ and the determination of Φ_{PC} will be more sensitive to the statistical model contribution when coverage of the measurements is not sufficient to fix the total potential variation. For example, when the coverage spans the dusk sector, Φ will be in reasonable agreement with the observations in the dusk convection cell, while Φ will be determined mostly by the model pattern in the dawn cell. The solution of Φ will thus be undesirably dependent on the choice of statistical model. This situation preserves the uncertainty characteristic of earlier studies of Φ and Φ_{PC}.

3. Analysis

The networks of HF coherent backscatter radars known as SuperDARN measure ionospheric LOS Doppler velocities over a large portion of the Northern and Southern Hemispheres [*Greenwald et al.*, 1995]. The northern component of SuperDARN has recently been augmented with two new radars in British Columbia, Canada, and Kodiak Island, Alaska. The additional radars extend the coverage of the network to include western North America (see Figure 1 and Table 1). This study focuses on a particular period during which SuperDARN measurements were available over a region of the Northern Hemisphere that extended over ~18 hours of magnetic local time (MLT) or nearly 3/4 of the high-latitude ionosphere.

In order to demonstrate that definitive global solutions of Φ are now possible with direct measurements of convection, we show that given sufficient coverage, as in the case for the period selected, the solution of Φ is insensitive to the selection of statistical model data. The fitting technique, further explained in the text, used to construct a global solution of Φ over the region $>50°\Lambda$,

Figure 1. Locations and fields of view of the eight operating SuperDARN HF radars in the Northern Hemisphere. Flags indicate the primary source of support of each radar. Radar identification letters are defined in Table 1.

is applied to the SuperDARN data in combination with a wide variety of statistical model patterns. The lack of any significant differences in the resulting solutions of Φ demonstrates that Φ and hence Φ_{PC} are largely constrained by the measurements alone.

3.1. Example of Fitting Technique

Figure 2 shows the LOS velocity data from all seven operational SuperDARN radars in the Northern Hemisphere during a standard 2 min scan from 1924 to 1926 UT on January 12, 2000. This period occurred before the Prince George radar was operational. The LOS data from each radar have been mapped into a grid of geomagnetic coordinates described by *Ruohoniemi and Baker* [1998]. Each grid cell containing data shows the average velocity for each radar contributing to the cell. The velocity magnitude is represented by the gray level of the dot that marks the cell location, and the direction is indicated by a tail on the dot that points in the direction of the observed flow. LOS Doppler measurements for this period are observed at >60°Λ and from ~0700 to 2400 MLT, encompassing roughly 3/4 of the convection zone.

The LOS Doppler measurements can be used to construct a global solution of the electrostatic potential. Figure 3 shows fitted velocity vectors and potential contours derived from the LOS measurements shown in Figure 2 using the technique described by *Ruohoniemi and Baker* [1998] with two improvements described in Appendix A. The fitting of the potential was carried out to order 8 ($L = 8$) in the spherical harmonic expansion (see Appendix A for an explanation of the fitting order), and the APL model corresponding to IMF magnitude $6 \leq B_T \leq 12$ nT and IMF orientation B_z-/B_y- was chosen to augment the LOS data.

Observations from a solar wind monitoring satellite, ACE, indicated that the IMF conditions impacting the magnetopause during this period were ~6 nT with roughly equal B_z- and B_y- components. The fitted velocity vectors in Figure 3 describe a pattern consisting of two large-scale convection cells in the dawn and dusk sectors, which is typical of periods of southward IMF [e.g., *Heppner and Maynard*, 1987]. The moderate to large flow velocities, generally ≤1 km/s with some areas >1 km/s, and significant potential variations, 27 kV across the dawn cell and 34 kV across the dusk cell, suggest that a moderate to strongly southward IMF condition exists at the dayside magnetopause. The effect of the observed IMF B_y- condition is evident in the strong (>1 km/s) duskward flow across the noon meridian near 78°Λ, which is part of a sharp rotation of flows in the postnoon sector [*Heppner*, 1972; *Heelis*,

Table 1. SuperDARN Radars Operating in the Northern Hemisphere

Radar	ID	Location	Affiliation	Lat.°N	Lon.°E	Operational	
CUTLASS[a]/Finland	F	Hankasalmi, Finland	University of Leicester	62.32	26.61	April	1995
CUTLASS[a]/Iceland	E	Pykkvibær, Iceland	University of Leicester	63.77	-20.54	Dec.	1995
Iceland West	W	Stokkseyri, Iceland	CNRS[b]	63.86	-20.02	Oct.	1994
Goose Bay	G	Labrador, Canada	JHU/APL[c]	53.32	-60.46	June	1983
Kapuskasing	K	Ontario, Canada	JHU/APL[c]	49.39	-83.32	Sept.	1993
Saskatoon	T	Saskatchewan, Canada	University of Saskatoon	52.16	-106.53	Sept.	1993
Prince George	B	British Columbia, Canada	University of Saskatoon	53.98	-122.59	Mar.	2000
Kodiak	A	Kodiak Island, Alaska	UAF[d]	57.62	-152.19	Jan.	2000

[a]Co-operative United Kingdom Twin Located Auroral Sounding System.
[b]Centre National de la Recherche Scientifique.
[c]Johns Hopkins University Applied Physics Labratory.
[d]University of Alaska, Fairbanks.

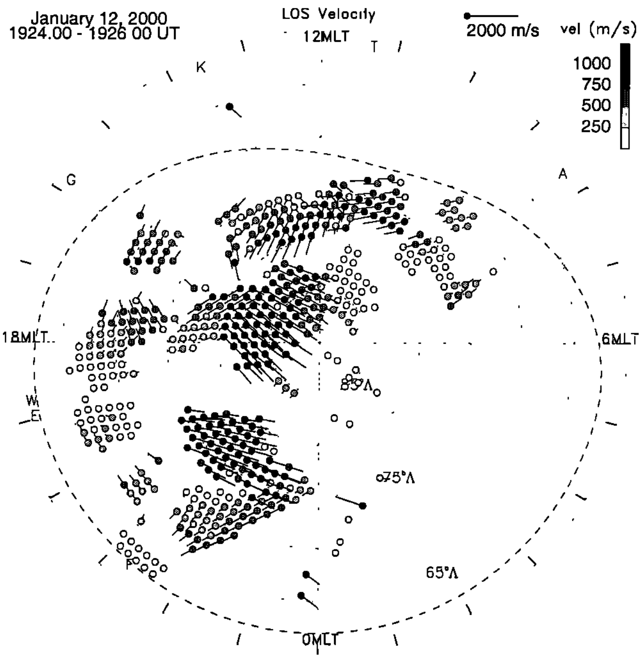

Figure 2. Line-of-sight (LOS) Doppler velocity data from seven SuperDARN HF radars in the Northern Hemisphere on January 12, 2000, 1924–1926 UT.

1984; *Greenwald et al.*, 1990]. Also, the larger and more circular dawn cell as compared to the more crescent shaped dusk cell suggests an IMF B_y- condition [e.g., *Reiff and Burch*, 1985; *Crooker*, 1979]. The pattern is quite similar to the DE model of *Heppner and Maynard* [1987] for IMF B_y- conditions, particularly in the dayside.

While the features of the convection pattern for this period are consistent with the IMF $6 \leq B_T \leq 12$ and B_z-/B_y- APL model, there are significant differences. Figure 4 shows grayscale shaded potential contours with dark dots marking grid cells that contain LOS measurements. The fitted pattern from Figure 3 is reproduced in Figure 4a for comparison with the statistical model data shown in Figure 4b.

The convection patterns in Figures 4a and 4b are similar in the largest-scale features, the two-cell morphology, and Φ_{PC}. Potential variations in the dawn and dusk cells are 27 kV and −34 kV ($\Phi_{PC} = 61$ kV), respectively, for the fitted patterns and −33 kV and 28 kV ($\Phi_{PC} = 61$ kV), respectively, for the statistical model data. Several interesting differences exist between these potential patterns. The largest difference in the patterns occurs in the dayside, where the throat region, located in the prenoon sector of the statistical data, is rotated to the postnoon sector in the fitted solution. The resulting dawn cell in the fitted solution extends much farther into the dusk region (~1500 MLT) than the statistical model data predicts. In addition, the dusk cell of the fitted pattern has two regions of large negative potential that extend over a broader range of MLT than shown in the statistical pattern.

Figure 4c shows the residual potential, which we define as the difference in the potential shown in Figures 4a and 4b, in this case the change from the statistical pattern to the fitted pattern. Note that the grayscale levels used in all of the residual potential plots are different by a factor of 2 from those used in the plot of the potential solutions to dramatize changes or lack thereof. The residual potential in Figure 4c shows that the largest differences between the two patterns occur in a region of the dayside between the MLTs where the throat is located in the two patterns and the premidnight sector, into which the dusk cell of the fitted pattern extends. The existence of large residuals (~35 kV) demonstrates that the LOS Doppler measurements determine the solution in these regions.

Smaller-scale features present in the fitted pattern (Figure 4a) but absent from the statistical model (Figure 4b) are due in part to the lower-order (6) fit used by *Ruohoniemi and Greenwald* [1996] in constructing the statistical patterns and to the tendency of statistical constructions to supress finer-scale features.

3.2. Sensitivity to Model Choices

The purpose of this study is to demonstrate that during periods when SuperDARN velocity measurements are available over a large portion of the convection zone the particular choice of statistical model has little effect on the resulting global potential pattern. By way of example, we perform the fitting technique using

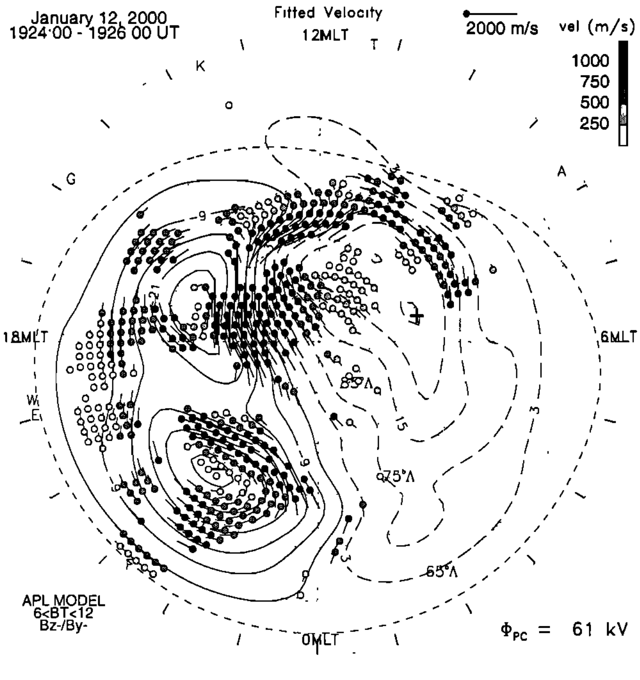

Figure 3. Fitted velocity vectors and electrostatic potential contours from the LOS measurements in Figure 2 using the technique described by *Ruohoniemi and Baker* [1998] to order 8 with the APL model for IMF magnitude $6 \leq B_T \leq 12$ nT, IMF orientation B_z-/B_y-, and the improvements discussed in Appendix A.

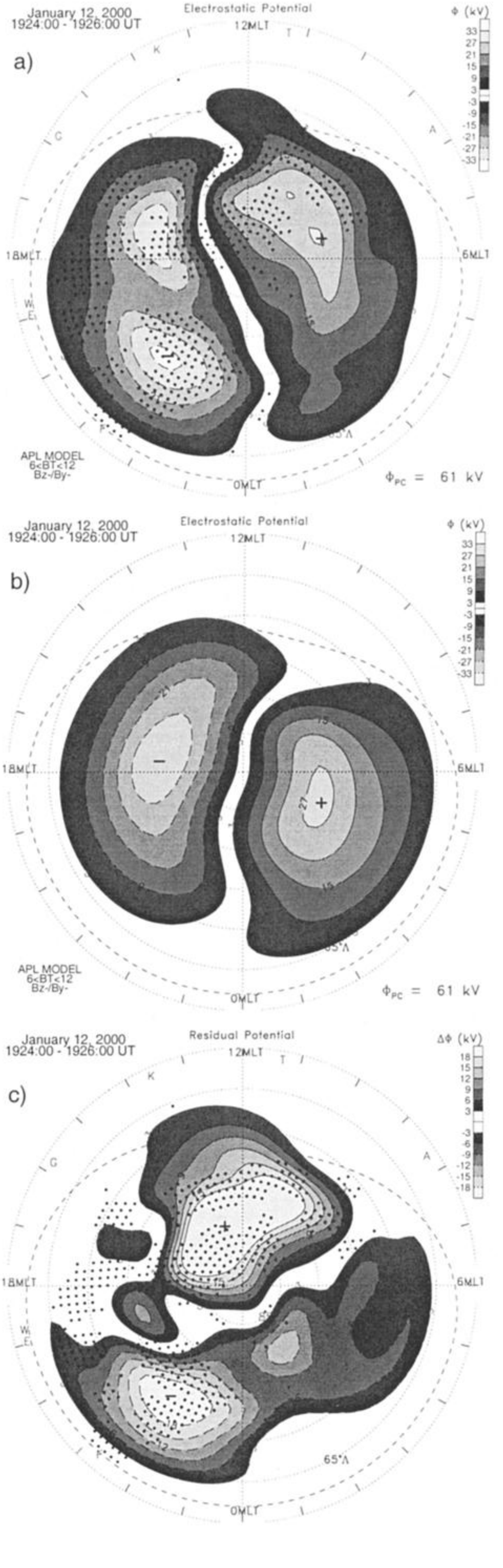

the APL model statistical patterns for IMF magnitude $6 \leq B_T \leq 12$ nT and each of the eight IMF orientations [*Ruohoniemi and Greenwald*, 1996, Figure 7]. The patterns are then compared to the solution obtained using the reference model (Figures 3 and 4a), and the differences are attributed to the statistical models used in the fittings.

Figure 5 shows residual potential contours for fittings using the APL model for the eight different IMF orientations illustrated compared with the reference solution. As expected, the largest change in potential is evident in the comparision with the IMF B_z+ model. The APL statistical model for this IMF orientation and magnitude range is most different from the B_z-/B_y- model used in the fitting. The dawn cell for the B_z+ model is virtually nonexistent and contains only 3 kV of potential variation, while the dusk cell is very contracted and contains 12 kV, resulting in $\Phi_{PC} = 15$ kV, as compared to $\Phi_{PC} = 61$ kV for the reference model (Figures 3 and 4a). Any change in the global solution due to the statistical model data should be obvious in the comparision between the fittings using these two models.

Figure 5b shows a region in the postmidnight/dawn sector where the residual potential is the largest. The region is located over northern Siberia and is characterized by only a few isolated LOS Doppler measurements from the farthest range gates of the radar network. The maximum residual potential in this region is ~11 kV. While it is true that the model vectors influence the solution in this area, the effect is small, localized, and entirely expected in a region with only statistical data available to define the solution.

The residual potential in regions where velocity measurements exist is only a few kV or less and limited to a small region in the postnoon/dusk sector, which is the throat region and has structure that the model patterns cannot reproduce. The global solution is therefore well-defined by the measurements in this instance. Only nominal variations in the patterns exist at mesoscale and smaller orders mainly in the regions where the drastically different statistical models are used to guide the solution. The residual potential plots in Figures 5a and 5c-h, using the other statistical models, show even less deviation from the reference pattern.

The APL statistical convection patterns, as defined by *Ruohoniemi and Greenwald* [1996], are also sorted by three categories of IMF magnitude: $0 \leq B_T \leq 4$ nT, $4 \leq B_T \leq 6$ nT, and $6 \leq B_T \leq 12$ nT. Residual potential contours (not shown) resulting from the

Figure 4. Electrostatic potential contours for IMF magnitude $6 \leq B_T \leq 12$ nT and IMF orientation B_z-/B_y-: (a) order 8 fitted solution from Figure 3, (b) APL statistical model after *Ruohoniemi and Greenwald* [1996], and (c) the residual potential of Figure 4a and Figure 4b, $\Delta\Phi$. Note the different grayscale levels for Figure 4c).

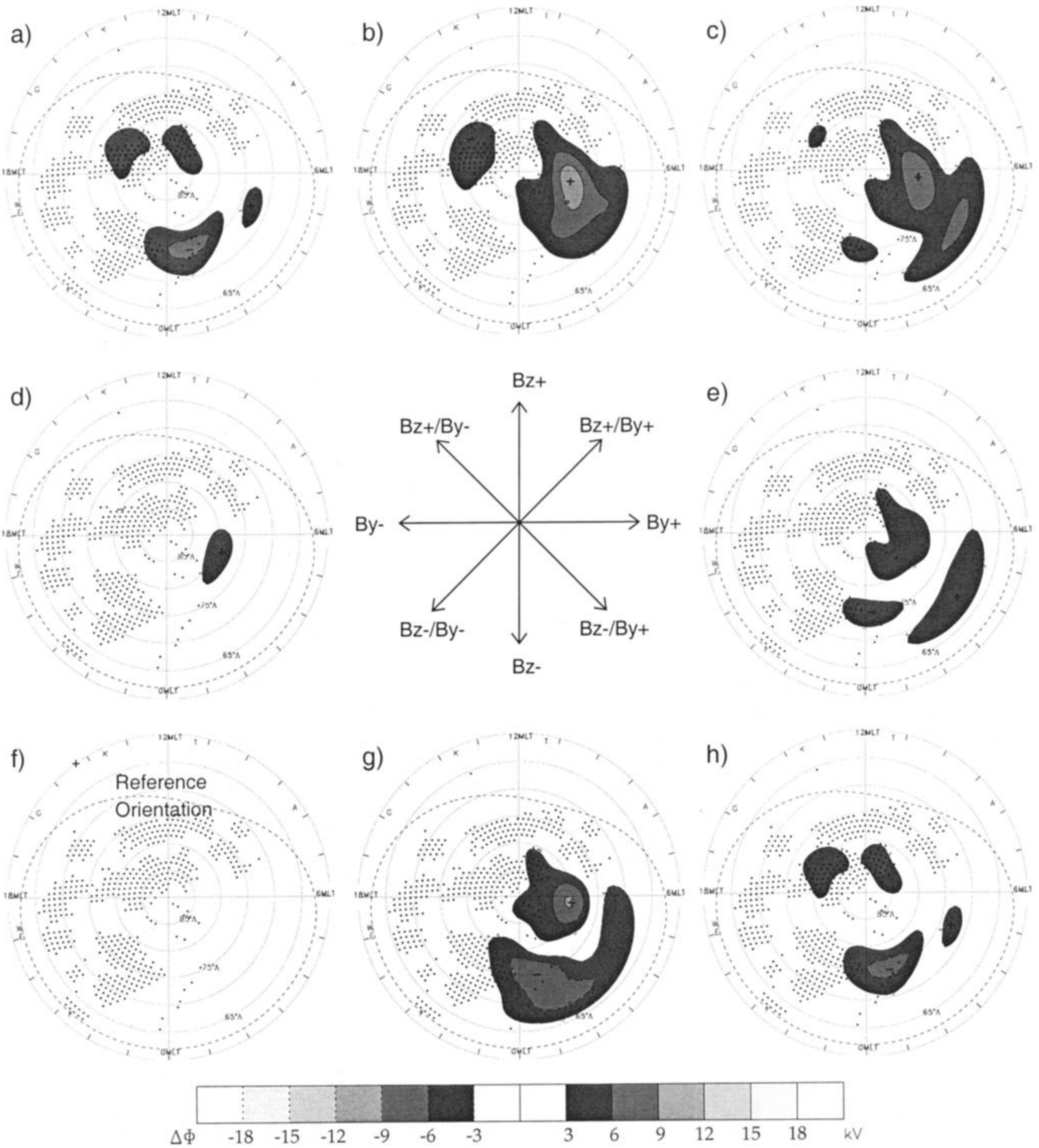

Figure 5. Contour maps showing the residual electrostatic potential for APL statistical models corresponding the IMF orientation indicated by the location of the plot. The reference pattern is computed using the APL model corresponding to IMF orientation B_z-/B_y-, shown in Figures 3 and 4a.

comparison of the reference solution (Figures 3 and 4a) and the fitted pattern using the same IMF orientation but IMF magnitude $0 \leq B_T \leq 4$ nT show only minor variations of less than a few kV in potential present only in the largest region that is lacking velocity measurements. The general features of the APL statistical models tend to scale with the IMF magnitude, so the effects of changing the model on the basis of IMF magnitude alone are minor and limited to regions containing only statistical data.

While there is minor mesoscale variation of the convection pattern due to different model selection, the total potential variation across the polar cap, Φ_{PC}, is remarkably constant regardless of the chosen statistical model. The range of Φ_{PC} for the fitted patterns is only 56–61 kV, while Φ_{PC} varies in the statistical patterns from 15 to 77 kV. Clearly, the LOS measurements during this period adequately constrain the determination of Φ_{PC}.

It is instructive to consider the reason for the insensitivity of the Φ_{PC} determination to the selection of statistical model data. The area of observations apparently encompasses the positions of the potential extrema and the flows in the intervening region. Thus the total potential variation is fixed by the observation of convection velocity through the polar cap. This important characteristic is reproduced by the fitting regardless of the nature of the sparse model data used to constrain the global solution. We can anticipate making definitive estimates of Φ_{PC} when this condition prevails. Most often, this will be realized when observations extend across much of the dayside region, as in this case.

We demonstrate how incompleteness in this coverage introduces a measure of ambiguity in the solution. We repeat the fitting but exclude Goose Bay data, which bridged an important portion of the postnoon convection pattern (see Figure 3). The larger dots in Figure 6b represent the grid cells at which the Goose Bay radar contributes LOS measurements. These cells occur between the dawn and dusk cells just poleward of the throat region, where large flow velocities are seen across the dawn-dusk meridian in Figure 3.

Figure 6a shows the potential pattern that results when these critical measurements are missing. Large residual potentials (~20 kV) are shown in Figure 6b resulting from comparing the pattern achieved using all the LOS data (Figure 4a) and that obtained without the Goose Bay data (Figure 6a). The potential across both cells is dramatically reduced without the Goose Bay data, resulting in $\Phi_{PC} = 43$ kV, far less than that obtained by fitting all the radar data with any choice of statistical model. The sensitivity to the selection of statistical model data is a consequence of the insufficiency of the measurements (without the Goose Bay radar) to fix Φ_{PC}.

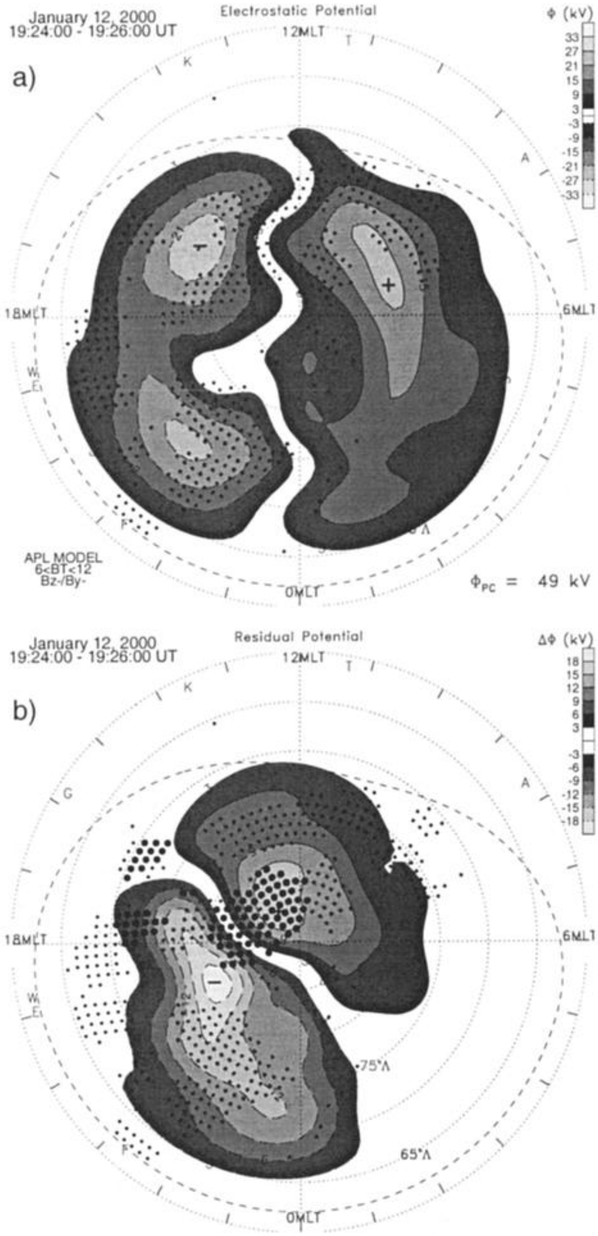

Figure 6. (a) Electrostatic potential contour map derived using the same IMF model as Figure 4a but without using the LOS data from the Goose Bay radar (b) and the resulting residual potential from Figures 4a and 6a. Larger dots represent grid cells where the Goose Bay radar contributes data.

4. Summary

To date, no technique exists for unambiguously mapping the ionospheric electric potential over the entire high-latitude convection zone. The existing methods for approximating a global solution of Φ suffer from one or more shortcomings, including limited coverage of measurements, overreliance on statistical data, and uncertainties inherent in inverting indirect measurements. The continued expansion of the SuperDARN radar networks is, however, now allowing important characteristics of the global pattern to be reliably determined from direct measurements.

The addition of two HF radars in western North America has extended the region over which the six existing SuperDARN radars provide direct measurements of plasma convection in the high-latitude ionosphere. During periods when LOS Doppler data provide sufficient coverage, the selection of statistical model data has little impact on the estimation of the important, large-scale properties of the convection pattern, such as Φ_{PC}. The resulting maps of Φ describe the global nature of ionospheric convection yet retain the smaller-scale features dictated by the local measurements.

An example period chosen for the extended coverage of radar measurements illustrates the independence of the fitted solution of Φ on the statistical models. Using the fitting technique of *Ruohoniemi and Baker* [1998] with two improvements discussed in Appendix A, maps of Φ constructed with statistical models that differ greatly in character show only minor variations. During such periods, Φ and Φ_{PC} are largely determined by the observations alone.

An important threshold has now been reached; namely, it is now possible to reliably map Φ and determine Φ_{PC} using direct measurements. During the example period only seven of the eight operational radars provided measurements of the convecting ionspheric plasma. Additional measurements from the new radar in British Columbia and another currently being constructed in Alaska will only add further confidence to Φ and Φ_{PC} obtained from this fitting proceedure. The product of this analysis will provide valuable checks of ionospheric quantities derived from global magnetospheric MHD models and concepts in SW-M-I coupling.

Appendix: Modifications of APL Global Convection Mapping Technique

Two modifications have been made to the mapping technique of *Ruohoniemi and Baker* [1998]. The fitted convection patterns now produced by the APL group, including those presented in this paper, incorporate these modifications unless otherwise specified. Here we describe the changes and the reasons for adopting them.

The first concerns the specification of the equatorward boundary of the convection zone. In *Ruohoniemi and Baker* [1998] this boundary, referred to here as Λ^{circ}, was taken to be a circle of constant invariant latitude. We use the value of Λ^{circ} at midnight MLT, $\Lambda_0^{\mathrm{circ}} \equiv \Lambda^{\mathrm{circ}}(0000\ \mathrm{MLT})$, to identify this circular boundary. The actual value of $\Lambda_0^{\mathrm{circ}}$ was either set to a constant (usually 60°) or varied from scan to scan to accommodate the varying size of the convection zone. The equatorward boundary was specified as a circle in the derivation of the statistical convection model of *Ruohoniemi and Greenwald* [1996], and this has been the accepted convention in studies of this kind. However, we have found that the SuperDARN data invariably indicate that the convection boundary is located at higher latitudes on the dayside than on the nightside. The definition of the boundary used in the fitting should reflect this character. As a practical matter, we have found that using a circular boundary that accommodates the flow on the nightside allows the flow on the dayside to extend to unrealistically low latitudes.

The solution is to introduce an MLT dependence in the specification of the boundary latitude. We have explored several options for the boundary, including a global shifting of the coordinate flows so that the convection pattern is centered on a point 4° equatorward of the magnetic pole toward the nightside. In the end, we adopted a solution based on the work of *Heppner and Maynard* [1987]. These authors studied the dependence of the latitude of the boundary on MLT and geomagnetic activity level using electric field measurements from the DE satellite. Their Figure 10 indicates that this boundary, referred to here as Λ^{HMB}, has a similar shape through all activity levels but expands and contracts. Figure A1 shows several examples of Λ^{HMB} boundaries for varying sizes of the convection zone. The boundary is almost circular on the nightside but rises steeply in latitude after crossing the dawn and dusk meridians, reaching a highest latitude near the 1100 MLT meridian. We characterize the size of the boundary by referring to the latitude of its intercept with the midnight MLT meridian, $\Lambda_0^{\mathrm{HMB}} \equiv \Lambda^{\mathrm{HMB}}(0000\ \mathrm{MLT})$. For a given scan, a value of Λ_0^{HMB} is determined such that all of the significant convection observations are contained within the boundary. Some freedom remains in choosing the limit to what defines significant flow, but 100 m/s is a typical value.

The spherical harmonic fitting continues to be performed over the entire region poleward of $\Lambda_0^{\mathrm{circ}}$, where, numerically, $\Lambda_0^{\mathrm{circ}} = \Lambda_0^{\mathrm{HMB}}$. Grid cells in the crescent-shaped region on the dayside located between the lati-

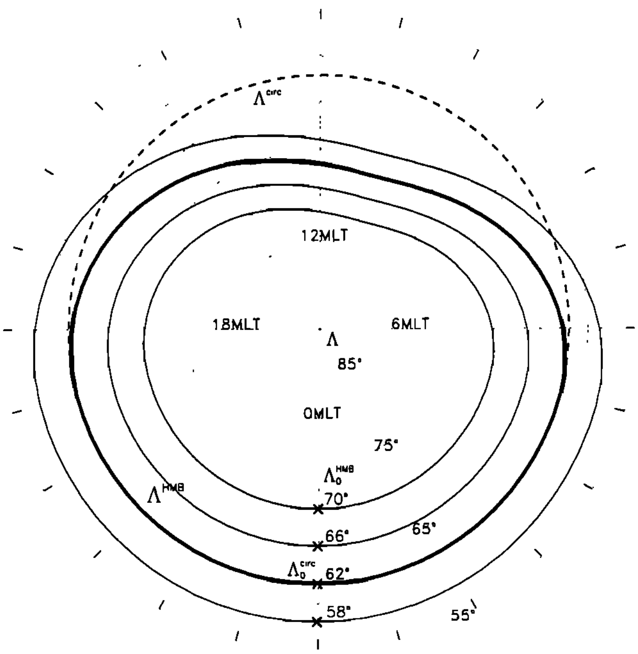

Figure A1. Examples of lower-latitude convection boundaries used in the improved fitting algorithm of *Ruohoniemi and Baker* [1998]. Four boundaries, Λ^{HMB}, based on the work of *Heppner and Maynard* [1987] are shown for midnight MLT latitude intersections of $\Lambda_0^{\mathrm{HMB}} = 58°, 62°, 66°$, and $70°$. The thick curve indicates the Λ^{HMB} boundary used in the fittings presented in this paper. The dashed line shows the circular boundary Λ^{circ}, defined by $\Lambda_0^{\mathrm{circ}} = 62°$, used in previous studies [e.g., *Ruohoniemi and Greenwald*, 1998].

tude of Λ^{circ} and Λ^{HMB} (see Figure A1) are padded with zero velocity vectors. Our implementation of Λ^{HMB} allows some small, but nonzero, potential contours to exist equatorward of the HMB boundary (see, for example, Figure 3). The resulting patterns more closely reproduce the character of convection at lower latitudes.

A consequence of using the lower-latitude convection boundary defined by Λ^{HMB} is a minor difference in the statistical model data used in the fitting. A careful inspection of Figure 4b reveals subtle differences from the statistical model of *Ruohoniemi and Greenwald* [1996]. The patterns derived by *Ruohoniemi and Greenwald* [1996] were fitted using a circular lower-latitude convection boundary (Λ_0) corresponding to 60°Λ. When the fitting technique of *Ruohoniemi and Baker* [1998] is used, Λ_0 is determined by the extent of the LOS observations and the statistical model is scaled accordingly, thus modifying the pattern somewhat.

The second improvement over the original fitting technique described by *Ruohoniemi and Baker* [1998] is a weighting scheme that reduces the tendency for the statistical model data to dominate the global solution of Φ at higher-order fittings. By the order of the fitting we refer back to the expansion of Φ used by *Ruohoniemi and Baker* [1998] in terms of spherical harmonic functions of order L and degree M. The values of L and M determine the resulting spatial filtering of the velocity data.

The original technique of *Ruohoniemi and Baker* [1998] weighted the statistical model data relative to the LOS velocity data without regard to the order of the fitting. The weight assigned to a velocity value from the model was set to the geometric mean of the radar velocity measurements. Fittings at higher order required progressively more statistical model vectors ($\propto L^2$) in order to constrain the behavior of the greater number of terms in the spherical harmonic expansion over the regions of no radar observations. A fixed weighting scheme therefore causes the solution to be more influenced by the statistical data at higher orders. The consequence was an undesirable compromise in selecting the order of the fitting at a level high enough to adequately reproduce finer-scaled features in areas where data were present but low enough so the statistical model did not dominate the solution.

An improvement has been made whereby the weight of the statistical data is adjusted according to the order of the fitting. The result is that the degree to which the model vectors affect the solution is less dependent on the order of the fit. In essence, the weight defined above as the geometric mean of the radar velocity measurements is reduced by the factor $4^2/L^2$. The effect is to roughly equalize the contribution of the statistical model to the fitting solution for $L \geq 4$ (fittings of order $L < 4$ are not considered useful). The cost associated with this progressive deweighting might be the emergence of erratic behavior in the patterns over the areas of no radar observations. However, we have found

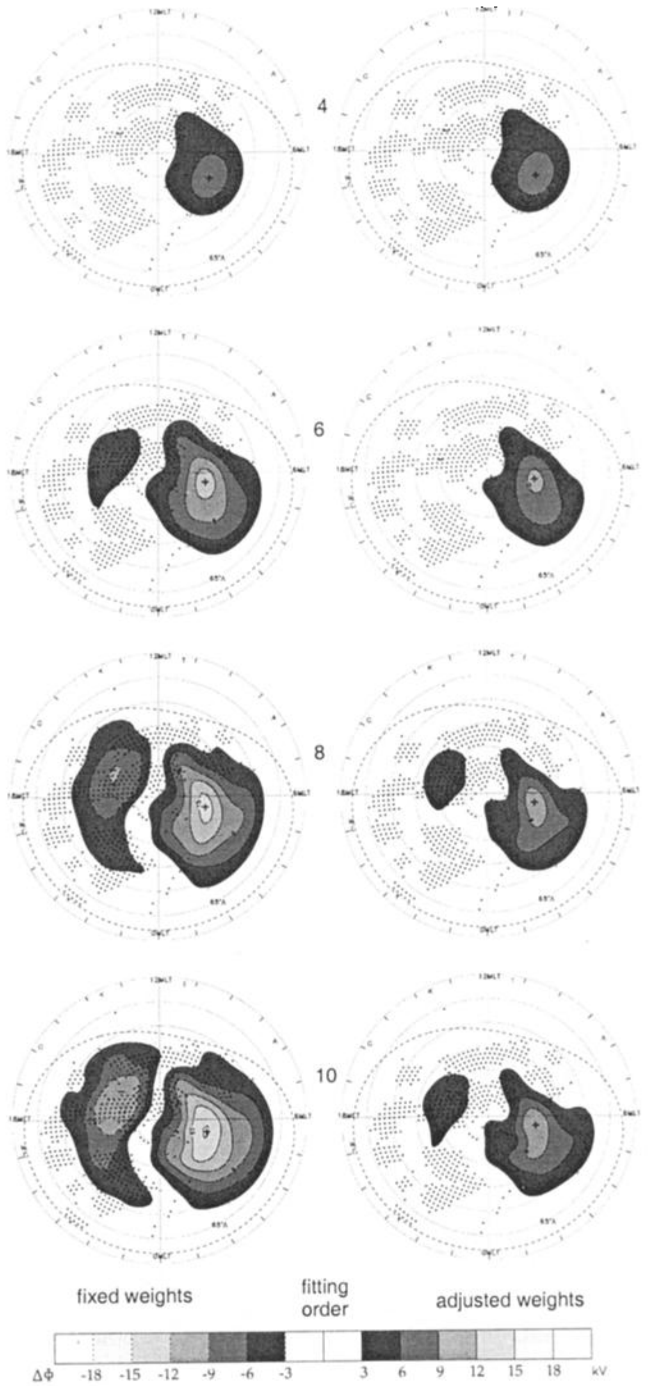

Figure A2. Residual electrostatic potential contours for order L = 4, 6, 8, and 10 fittings (top to bottom) using fixed and adjusted weights (left and right columns) for the statistical velocity data. The two APL models used to obtain the residuals correspond to IMF orientation B_z-/B_y- and B_z+ with IMF magnitude $6 \leq B_T \leq 12$ nT for both fittings.

the results to be quite satisfactory with these settings, at least up to fittings of order L = 10. Higher-order fittings can now be used to reproduce smaller-scale features described by the LOS measurements, and the statistical model data simply guide the solution realistically in regions where no radar data are available.

Figure A2 shows residual potentials for varying orders of fit (L = 4, 6, 8, and 10 from top to bottom) for both the fixed and varied (left and right column) weighting schemes. Inspection of the residuals in the left column of Figure A2 shows the problem of using a high-order fit with the fixed weighting scheme of *Ruohoniemi and Baker* [1998]. Increasingly large (>12 kV) residual contours are evident as the order is increased. In this example the increasing fitting order is inadvertently causing the global solution to converge on the solution defined by the statistical model.

The right column of Figure A2 reveals a slight trend toward larger residuals with increasing fitting order, implying that the statistical data is influencing the solution to a greater extent in the higher-order fittings. However, in regions where LOS velocity data are present (e.g., 1500–1800 MLT and 75–85°Λ), the maximum deviation in the residual is less than or equal to ~3 kV. Such minor change in the residual contours from order 4 to 10 demonstrates that the improved weighting scheme allows the fitting technique to be virtually independent of order in regions were velocity data are present. Larger residual deviations (up to ~10 kV) are seen in the postmidnight/dawn region where no velocity measurements exist. Such a trend is expected at higher orders. The additional statistical data used in the higher-order fittings cause the differences between model patterns to become more evident in locations where no data exist.

Contrasting the right column in Figure A2 with the left column shows the marked improvement the adjusted weighting scheme has on reducing the impact of the statistical model at higher orders. Smaller-scale features present in the velocity data can now be reproduced in the global patterns without significant influence from the statistical model data.

Acknowledgments. This work was supported by NSF grant ATM-9812078 and NASA grant NAG5-8361. Operation of the Northern Hemisphere SuperDARN radars is supported by the national funding agencies of the U.S., Canada, the U.K., and France. We gratefully acknowledge the CDAWeb for access to the ACE solar wind data.

Janet G. Luhmann thanks John D. Kelly and C. Robert Clauer for their assistance in evaluating this paper.

References

Boyle, C. B., P. H. Reiff, and M. R. Hairston, Empirical polar cap potentials, *J. Geophys. Res.*, *102*, 111, 1997.

Crooker, N. U., Dayside merging and cusp geometry, *J. Geophys. Res.*, *84*, 951, 1979.

Greenwald, R. A., K. B. Baker, J. M. Ruohoniemi, J. R. Dudeney, M. Pinnock, N. Mattin, J. M. Leonard, and R. P. Lepping, Simulataneous observations of dynamic variations in high-latitude dayside convection due to changes in IMF B_y, *J. Geophys. Res.*, *95*, 8057, 1990.

Greenwald, R. A., et al., DARN/SUPERDARN: A global view of the dynamics of high-latitude convection, *Space Sci. Rev.*, *71*, 761, 1995.

Heelis, R. A., The effects of interplanetary magnetic field orientation on dayside high latitude ionospheric convection, *J. Geophys. Res.*, *89*, 2873, 1984.

Heppner, J. P., Polar-cap electric field distributions related to the interplanetary magnetic field direction, *J. Geophys. Res.*, *77*, 4877, 1972.

Heppner, J. P., Empirical-models of high-latitude electric-fields, *J. Geophys. Res.*, *82*, 1115, 1977.

Heppner, J. P., and N. C. Maynard, Empirical high-latitude electric field models, *J. Geophys. Res.*, *92*, 4467, 1987.

Reiff, P. H., and J. L. Burch, IMF B_y-dependent plasma flow and Birkeland currents in the dayside magnetosphere: A global model for northward and southward IMF, *J. Geophys. Res.*, *90*, 1595, 1985.

Reiff, P. H., R. W. Spiro, and T. W. Hill, Dependence of polar cap potential drop on interplanetary parameters, *J. Geophys. Res.*, *86*, 7639, 1981.

Richmond, A. D., and Y. Kamide, Mapping electrodynamic features of the high-latitude ionosphere from localized observations: Technique, *J. Geophys. Res.*, *93*, 5741, 1988.

Ruohoniemi, J. M., and K. B. Baker, Large-scale imaging of high-latitude convection with Super Dual Auroral Radar Network HF radar observations, *J. Geophys. Res.*, *103*, 20,797, 1998.

Ruohoniemi, J. M., and R A. Greenwald, Statistical patterns of high-latitude convection obtained from Goose Bay HF radar observations, *J. Geophys. Res.*, *101*, 21,743, 1996.

Ruohoniemi, J. M., and R. A. Greenwald, The response of high-latitude convection to a sudden southward IMF turning, *Geophys. Res. Lett.*, *25*, 2913, 1998.

Slinker, S. P., J. A. Fedder, B. A. Emery, K. B. Baker, D. Lummerzheim, J. G. Lyon, and F. J. Rich, Comparison of global MHD simulations with AMIE simulations for the events of May 19–20, 1996, *J. Geophys. Res.*, *104*, 28,379, 1999.

Weimer, D. R., Models of high-latitude electric potentials derived with a least error fit of spherical harmonic functions, *J. Geophys. Res.*, *100*, 19,595, 1995.

J. M. Ruohoniemi and S. G. Shepherd, The Johns Hopkins University Applied Physics Laboratory, 11100 Johns Hopkins Road, Laurel, MD 20723. (mike.ruohoniemi@jhuapl.edu; simon.shepherd@jhuapl.edu)

(Received May 11, 2000; revised July 13, 2000; accepted July 13, 2000.)